CrossMark

ORIGINAL PAPER

Adhesion and Friction Enhancement of Film-Terminated Structures against Rough Surfaces

Zhenping He[1] · Nichole M. Moyle[1] · Chung-Yuen Hui[2] · Benjamin Levrard[3] ·
Anand Jagota[1,4]

Abstract A number of biomimetic and bioinspired micron-scale surface structures have been developed in recent years with unique surface properties such as highly enhanced and switchable adhesion and friction against smooth surfaces. However, few studies have examined the effect of roughness on mechanisms for property enhancement, although this is of critical importance for applications. Here, we investigate the effect of roughness on adhesion and friction of a family of film-terminated fibrillar and ridge/channel microstructures. Although increasing roughness uniformly attenuates adhesion and friction, we find that the film-terminated structures maintain their enhancement compared to flat controls against a variety of rough surfaces (including natural stones). The principal mechanisms underlying property enhancement against smooth surfaces remain operative against rough surfaces. We show how the effect of roughness on surface mechanical properties of structured surfaces can be understood as a combination of known effects due to structure and roughness.

✉ Anand Jagota
anj6@lehigh.edu

1 Department of Chemical and Biomolecular Engineering, Lehigh University, D331 Iacocca Hall, 111 Research Drive, Bethlehem, PA 18017, USA

2 Department of Mechanical and Aerospace Engineering, Cornell University, Ithaca, NY 14853, USA

3 Michelin Corporation, European Center of Technologies, rue bleue ZI Ladoux, 63112 Clermont-Ferrand, France

4 Department of Bioengineering, Lehigh University, Bethlehem, PA, USA

1 Introduction

Inspired by the discovery of fine structures in the contacting surfaces of geckos and other small animals [1, 2], many groups have reported micro- and/or nanopatterning of surfaces as a successful strategy to achieve novel properties in adhesion [3–5] and friction [6, 7]. Various factors have been investigated to optimize the behavior of structures with patterns on their surface, such as their geometry [4, 5, 7–10]—pillars with flat or spherical caps, tubes and concave tips, spatulae, film-terminated structures, mushroom-shaped fibrils—and pattern parameters [6, 10–12] such as the height, diameter and spacing of features. To be useful, such materials need to maintain enhanced function against rough surfaces. It is well known that adhesion of elastic solids generally decreases with surface roughness [13], but it is not clear to what extent the mechanisms for adhesion or friction enhancement of biological and bioinspired patterned structures survive against rough surfaces. In the case of the gecko, its adhesion is weakened on surfaces with RMS roughness ranging from 100 to 300 nm [14], a range that matches the dimensions of its fine structure. Numerous reports have demonstrated the superior performance of patterned materials against smooth substrates [6, 8, 15–19]. However, research about how these properties fare on rough surfaces is still limited [15, 20–23]. Persson's theoretical work illustrates the dependence of fibril-array adhesion on substrate roughness [24]. Recent research on the contact between a fibrillar structure and rough glass surfaces shows that there is a link between the fibril diameter and certain characteristics of the roughness; adhesion enhancement is lost if fibril diameter is

smaller than a characteristic spacing between peaks in the roughness profile [16]. Kasem and Varenberg investigated the sensitivity of adhesion for mushroom-shaped microstructures (pillar height 100 μm and contacting plate diameter 50 μm) to roughness with relatively small $R_a < 2.3$ μm (R_a is the average absolute value of deviation of the surface profile from its mean), and introduced a new adhesion-oriented integrative roughness parameter [20]. Additionally, Burton and Bhushan [25] have pointed out the importance of dimension matching between contacting pairs of structured surfaces.

The decrease in contact area due to roughness and uneven strain distribution due to asperities contribute to the adhesion and friction reduction in elastomers on rough surfaces [26–28]. Several characteristics of a rough surface can be important in relating changes in adhesion or friction to roughness. For bulk elastic materials, adhesion and rolling resistance generally decrease with the increase in R_a [13]. For structured samples such as those with mushroom-shaped fibrils, the single parameter characterizing roughness, R_a, fails to explain how adhesion depends on characteristics of a structured surface. For surfaces comprising a pattern of pillars, the energy sacrifice due to accommodating pillars onto a rough surface (bending/buckling), and partial contact on pillar tips cause different effects of roughness [15, 16, 21, 23, 29]. It has been suggested that the 'Mean spacing between local peaks' [16] is a critical surface characteristic for adhesion, in addition to R_a or RMS roughness [15, 20, 22, 30].

Film-terminated fibrillar and ridge/channel structures show excellent capability in modulating adhesion and/or friction [11, 19, 31]; these are related to but different from fibrillar structures without a terminal film [6, 8, 18], such as mushroom-shaped structures. Such bioinspired structures have a nominally flat surface similar to bulk materials, with subsurface micropatterns. In particular, the mechanism for adhesion and static friction enhancement is crack-trapping, which means that the interfacial crack is trapped in regions between successive fibrils. For this reason, detachment is accompanied by periodic mechanical instabilities resulting in larger energy loss compared to an unstructured flat control. The influence of roughness on such structures, in particular on whether and how the crack-trapping mechanism is affected, is expected to be different from bulk and fibril-patterned materials. Here, we report on an investigation of how adhesion and static friction of film-terminated surfaces are altered against different rough substrates including laboratory-roughened glass and natural stones. We find that although the absolute value of adhesion and static friction reduce systematically with roughness (as characterized by the actual area of contact for a fixed load), their enhancement with respect to an unstructured flat control sample is substantially retained. For the film-terminated ridge/channel structures, an internal folding mechanism [32] for kinetic friction enhancement is retained against rough surfaces.

2 Experimental Section

Seven indenters were used in the experiments. One is a smooth glass indenter (labeled smooth), and three are roughened glass indenters (labeled as C1, F2 and P1). All four glass indenters were fabricated by melting a 2-mm glass rod in a propane flame. The radius of the glass indenters was about 3 mm; the stone indenters had a similar radius of curvature in the region of contact. Three of these indenters were roughened in a tumbler (NSI International Inc, item # 635) using different grit polishing media. The indenter C1 was made with "coarse grit," indenter F2 was made with "fine grit", and P1 with "pre-polish grit." The last three indenters, labeled S2, S3, and S4, were cut off from rounded corners of stones provided by the Michelin Corporation as typical of those used in road surfaces. All the glass indenters were coated with a self-assembled monolayer to reduce the surface energy, preventing sample damage and improving reproducibility of experimental data [5], while all the stone indenters were simply washed with de-ionized water and used without further treatment. The top left image in Fig. 1 shows these indenters.

The samples were fabricated using poly(dimethylsiloxane) (PDMS, Sylgard 184, Dow Corning) following the procedure of Glassmaker et al. [5]. Briefly, an array of periodic pillars or ridges was created by molding PDMS into a microfabricated silicon template. After being peeled off the silicon mold, the patterned PDMS substrate was placed on a partially pre-cured PDMS film with thickness controlled through spin coating. The assembly was then cured at 80 °C for 2 h. Two different structures were made: film-terminated ridge/channels and film-terminated fibrils as shown in Fig. 2. For the film-terminated ridge/channel structure, the samples were of ridge height D: 40 μm, film thickness h of about 10 μm and substrate thickness of about 700 μm. The periodic spacing between adjacent ridge centers was varied from 20 to 125 μm and denoted as S. For the film-terminated fibrillar structure, the samples were of fibrillar height D: 30 μm, film thickness h of about 10 μm and substrate thickness of about 700 μm. The spacing between adjacent fibrillar centers, S, was varied from 30 to 90 μm. A PDMS flat control sample was also fabricated under the same conditions. In the article, D30S90, for example, corresponds to a sample of structure height 30 μm and spacing 90 μm.

Several roughness characteristics of the indenter surfaces were measured in order to seek a correlation between adhesion and friction on the one hand and surface roughness on the other (see SI.1, Tables S1 and S2, for details). Although in all cases structured surfaces showed enhancement of adhesion and friction compared to flat controls, we found little systematic change in adhesion or static friction with roughness measure. The exception was the actual contact area of each indenter against a flat control sample

Fig. 1 Seven indenters used for friction and adhesion measurements. The top left of the figure shows a picture of the indenters. The remaining figures are images of the area of contact estimated by image analysis of micrographs of the contact region, as described in more detail in the text
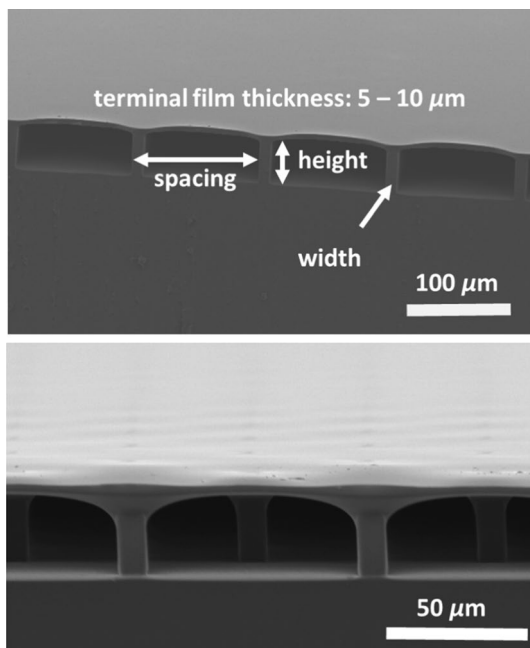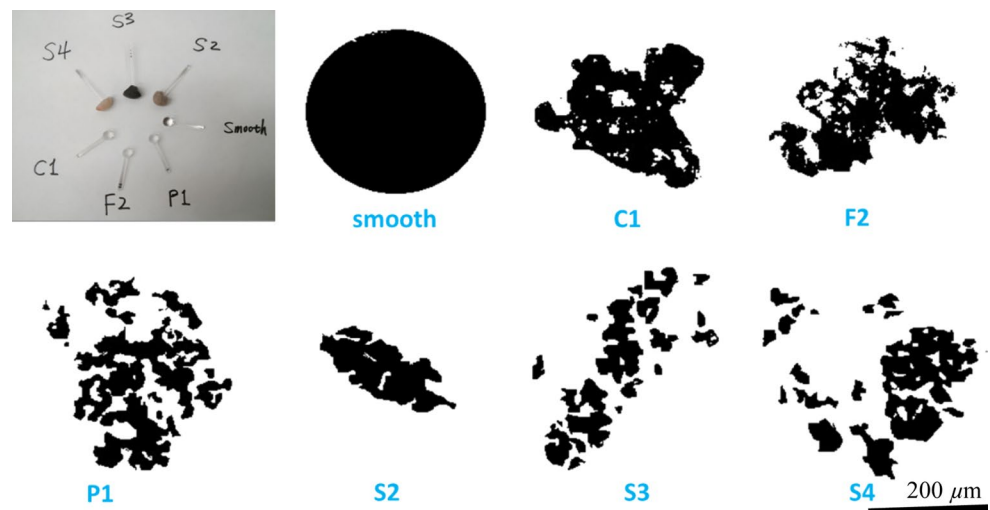

Fig. 2 (Top) Scanning electron micrograph of a film-terminated ridge-channel structure. (Bottom) Scanning electron micrograph of a film-terminated fibrillar structure

under a prescribed normal load (1 mN) *taken in same set of experiments in which all surfaces were tested*. The contact area was measured by converting optical micrographs into a binary image by setting a threshold intensity using the software ImageJ®. Figure 1 shows the result of this operation on each of the indenters. (The corresponding set of the original optical micrographs is shown in SI, Fig. S2.) Measured actual contact area for different indenters was normalized by the contact area of the smooth indenter, and we define the resulting quantity to be the contact roughness factor, α.

To measure friction under a controlled normal load, we used the apparatus and procedure described in SI (Fig. S3). Briefly, the indenter is brought into contact with a sample (supported on a glass slide) that is placed on an inverted microscope under a specified normal load controlled by a mechanical balance (Ohaus 310D). Then, the sample is driven by a variable speed motor (Newport ESP MFA-CC) at 5 µm/s. The frictional force is measured by a load cell (Honeywell Precision Miniature Load Cell), while the deformation is visualized and recorded through an inverted optical microscope. Measurements were performed for the film-terminated fibrillar and ridge/channel sample sets. For the ridge/channel structures, the indenter moved orthogonal to ridges. During friction measurement, the normal load was maintained at 1 mN. Selected results are present in the main manuscript; see SI for more details.

To measure adhesion we used the apparatus and procedure as shown in SI (Fig. S4). Typically, an indenter was mounted to a load cell (Honeywell Precision Miniature Load Cell), and the assembly motion was controlled by a motorized vertical stage. During the experiment, the indenter was first brought into contact with the sample, indented into the sample (15–30 microns, see Figure S5), and then withdrawn at a constant speed of 1 µm/s. A video of the contact region was captured by an inverted optical microscope. The adhesion, defined as the pull-off force, was evaluated based on the force signal recorded through the load cell.

3 Results and Discussion

3.1 Experimental Results

Figure 1 shows differences in actual area of contact for the different indenters on a flat control sample under 1 mN normal load. For the smooth indenter, the contact region is

regular and nearly circular. It is clear that for all the rough indenters contact is partial and often in separate regions. Since the same PDMS flat control sample and normal load were used for all the indenters, this contact area can serve as a quantitative proxy for the roughness of different indenters, i.e., the actual contact area is smaller for a rougher indenter and is a local measure of exactly the same contact region as used to measure adhesion and friction. (Measurement of contact roughness factor is described in SI.1.)

Figure 3a shows typical friction force–displacement plots for sliding the rough indenter F2 on four different film-terminated fibrillar structures and a flat control sample at a constant speed of 5 µm/s under normal load of 1 mN. In all cases, the structured samples show a characteristic peak in force, the static friction, which corresponds to the onset of sliding. The magnitude of the peak increases significantly with increasing separation between fibrils. (However, as we have shown previously [19], with

further increase in spacing, static friction reduces along with a change in mechanism.) The friction against the rough indenters is substantially reduced for the flat control as well as for the structured samples. However, it is clear that the strong enhancement of static friction previously shown for film-terminated fibrillar structures [19] is retained for rough indenter surfaces. For example, in Fig. 3a, the static friction of the flat control is 3.5 mN, whereas that for sample D30S90 is 15.4 mN, an enhancement by a factor of about 4.5.

Figure 3a inset shows the deformation in the contact region for film-terminated fibrillar sample D30S90 in contact with indenter F2 under normal load of 1 mN at the point where highest static friction was observed (red square). The red circle in Fig. 3a corresponds to the point where the friction force drops just after the point of highest static friction and sliding commences. We observe that the contact line moves slower between fibrils and faster when jumping over
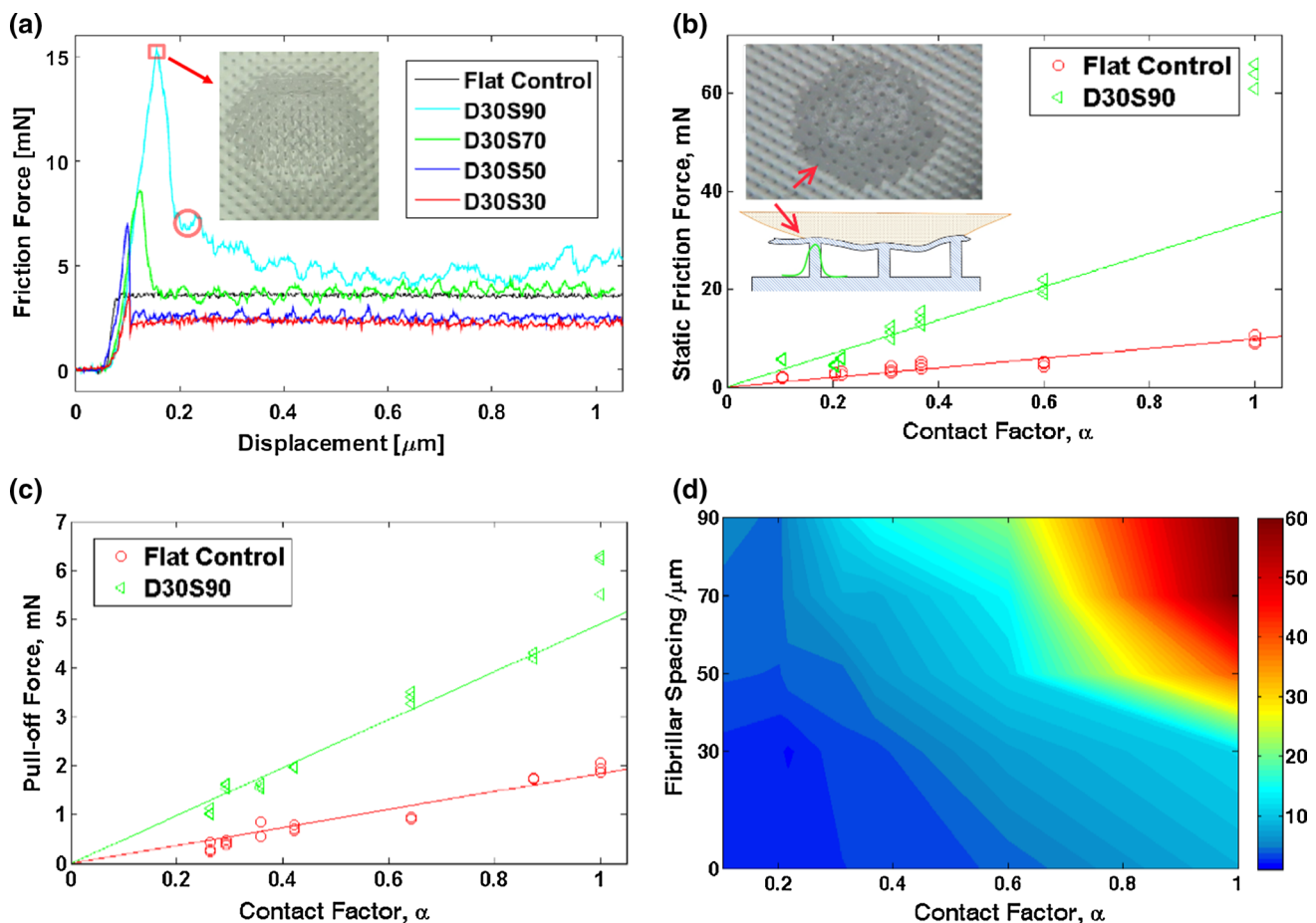

Fig. 3 **a** Force versus displacement during sliding of rough indenter F2 on a film-terminated fibrillar surface. The enhancement of static friction due to crack-trapping is retained against a rough surface. (Inset: optical micrograph of the contact region.) **b**, **c** Both static friction and adhesion, as measured by pull-off force, increase linearly with contact roughness factor. Inset in **b** shows an optical micrograph of the contact region during normal indentation. **d** Contour plot of static friction as a function of the contact roughness factor, α, and the fibrillar spacing for sample set of fibril height 30 µm. The colorbar represents static friction values in mN (Color figure online)

fibrils, consistent with a crack-trapping mechanism [5, 19] for static friction enhancement.

The static friction for flat control and film-terminated fibrillar sample D30S90 and its static friction enhancement ratio are shown in Fig. 3b (and Table. S3 in SI).

It has previously been shown that adhesion, as measured by the force required to pull-off a spherical indenter, is also enhanced by the crack-trapping mechanism [33]. Figure 3c plots the pull-off force for the film-terminated sample D30S90 as a function of contact roughness factor. With a decrease in contact area, the pull-off force decreases systematically, in a manner similar to static friction, reinforcing the idea that crack-trapping remains operative in both cases even with rough indenters. Typical force–displacement traces for samples with different fibrillar spacing using rough indenter C1 are plotted in SI Fig. S5. The clear trend in static friction and pull-off force with contact roughness factor confirms that it is an effective representative of sample roughness.

A systematic study of the effect of roughness and fibrillar spacing on static friction for the fibrillar samples is summarized in Fig. 3d. These data confirm that although decrease in contact roughness factor uniformly decreases static friction, the enhancement due to structure is retained.

The effect of rough indenters was also studied for the film-terminated ridge/channel structures which show significant ability to modulate sliding friction [32]. Figure 4a shows typical friction–displacement traces for indenter C1 moving orthogonal to ridges on film-terminated ridge/channel samples. Plots of force–displacement traces for different indenters on flat control and sample D40S125 are provided in SI (Fig. S6).) The results shown in Fig. 4a are similar to those reported with a smooth indenter. In particular, we observe strongly enhanced sliding friction for large spacing (125 microns) with periodic force oscillation tied to subsurface folding and sliding that is the cause of friction enhancement. The friction enhancement for sample D40S125 is about a factor of four, whereas samples D40S65 and D40S35 show decreased friction, again consistent with measurements against a smooth indenter. Figure 4b shows friction measurements for different indenters on D40S125, and friction enhancement ratio values are provided in SI Table S5. Because the internal folding mechanism for enhancement of sliding friction operates only for samples with largest spacing, we have focused on the spacing of 125 μm. The inset in Fig. 4 shows an image of the contact region during steady sliding of rough indenter C1 on sample D40S125, and the inset drawing illustrates the structural deformation that accompanies the friction enhancement.

Four of the indenters are made of the same glass, while the other three are stones of indeterminate surface composition. The indenters also have small variations in their radii. Despite this, there is a consistent overall trend of reduction in friction with decreasing contact roughness factor. The
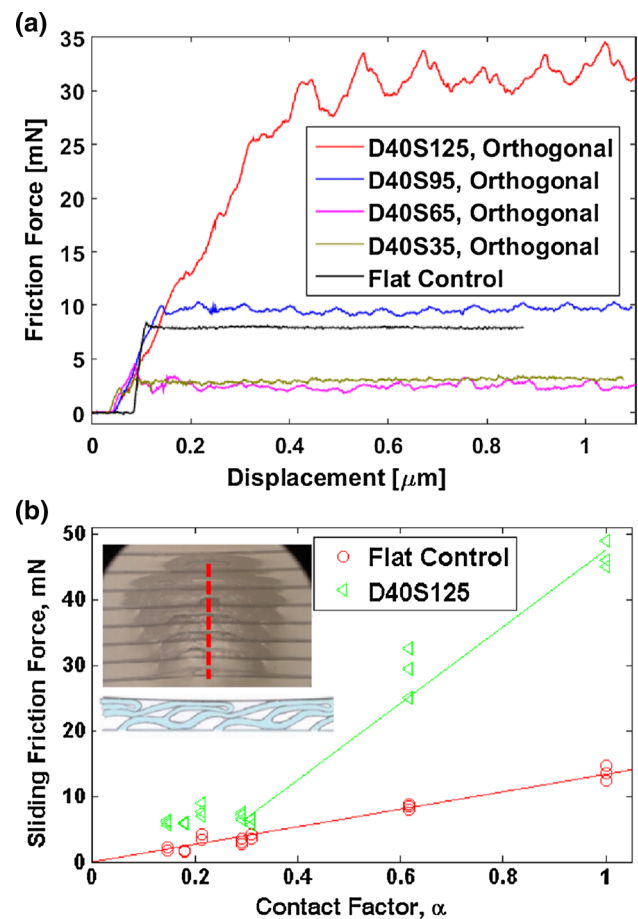

Fig. 4 a Force versus displacement for sliding a rough indenter C1 orthogonal to ridges in a film-terminated ridge-channel structure. **b** Sliding friction increases with contact roughness factor for both the structured samples and the flat control. (Inset: Optical micrograph of contact region and schematic deformation of the structures illustrating the friction enhancement mechanism of internal folding, stretching and sliding.)

various indenters, stones and glass, very likely are all combinations of inorganic oxides. Evidently, their intrinsic work of adhesion against PDMS does not vary much. In contrast, the contact roughness factor varies by about a factor of three. It thus appears that the effect of roughness is the principal determinant of relative measured properties. Figure S7 in SI shows that the internal subsurface deformation mechanisms that enhance sliding friction against a smooth surface remain at least partially operative against the rough indenters.

3.2 Interpretation

In order to understand the results just presented for adhesion and friction of a structured elastomer against a rough indenter, it is useful to identify two types of indenters, two types of surfaces, and their four combinations (Fig. 5): (a) smooth indenter on a flat elastomer; (b) rough indenter on a flat elastomer;
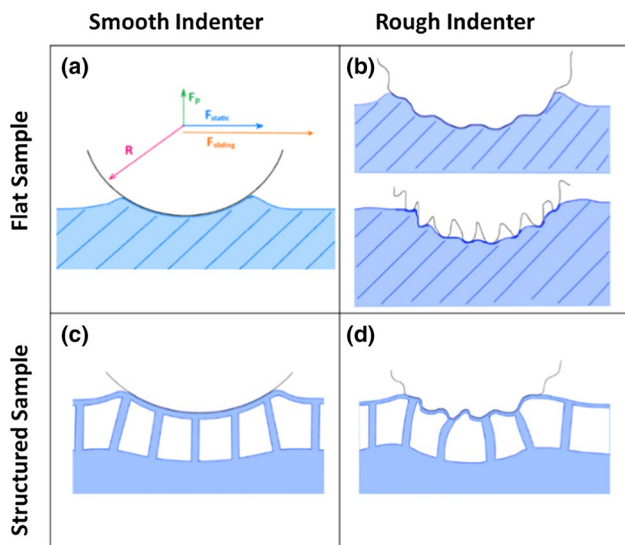
Fig. 5 Schematic representation of four cases resulting from a combination of smooth versus rough indenters and flat versus structured surfaces. Adhesion, static friction, and sliding friction are well understood for case (**a**), and reasonably well known for cases (**b**, **c**). Here, we are concerned with case (**d**), which we interpret in terms of our understanding of (**a–c**)

(c) smooth indenter on a structured elastomer, and (d) rough indenter on a structured elastomer. Case (a) is well understood; cases (b) and (c) are reasonably well studied. Case (d), which is of our interest, can then be understood as a departure from the better studied cases (a), (b), and (c).

Case (a) Adhesion and static friction for the contact pair of smooth indenter and flat soft solid are well understood, in the sense that the relationship between work of adhesion and pull-off force (under normal or shear load, respectively) is well known. Based on JKR [34] theory and its generalization by Savkoor and Briggs [35] to account for shear load, the pull-off force, F_p, and static friction, F_{static}, are both proportional to indenter radius, R, and work of adhesion, W:

$$F_p = \frac{3}{2}\pi RW \tag{1}$$

$$F_{static} = \sqrt{6\pi RW} \tag{2}$$

Steady sliding of a smooth indenter on a flat soft material is resisted by a characteristic constant interfacial shear stress [36], τ (typically between 100 and 200 kPa for PDMS). Thus, if A is the actual contact area, the sliding force is

$$F_{sliding} = \tau A \tag{3}$$

Case (b) When a rough indenter is placed on a soft solid, two different cases need to be considered. First, for a mildly

rough indenter, there is full contact between indenter and soft material (top image of Fig. 5b). In this case, for certain structured surfaces, effective interfacial adhesion can be enhanced due to crack-trapping instabilities [37, 38]. However, generally for randomly rough surfaces, the main effect is to introduce an additional elastic energy per unit area [27] (U_{el}), a penalty associated with local deformation required to make the two surfaces conform to each other. This energy is released as the interface opens, and therefore the work of adhesion, W_r, is reduced from its value for a flat surface (ignoring the relatively modest increase in area due to the roughness).

$$W_r = W - U_{el} \tag{4}$$

Evidently, W_r is smaller than W and replaces it in Eqs. (1) and (2).

In the second case, the material cannot deform enough to achieve full contact with the rough indenter (bottom image of Fig. 5b). Equations (1) and (2) are both based on the assumption of full contact. The effect of partial contact has been studied widely [35, 39–41]. Generally, contact area decreases for rougher surfaces and so does the pull-off force and static friction. One can approximately write the effective work of adhesion as

$$W_{r,eff} = \alpha(W - U_{el}), \tag{5}$$

where α is the contact roughness factor, the ratio of contact area of rough indenter to the contact area of smooth indenter. (Assuming that the extra elastic energy associated with the roughness is also proportional to the actual contact area.) Substituting Eq. (5) for W in Eqs. (1) and (2) yields the prediction that both pull-off force and static friction should increase in proportion to the actual contact area. This prediction is consistent with data on the flat control shown in Fig. 3b, c. In addition, Eq. (3) predicts that sliding friction should also be proportional to actual contact area, which is consistent with the data shown in Fig. 4b (flat control).

Case (c) For film-terminated fibrillar samples, we have previously established that the adhesion is enhanced due to a crack-trapping mechanism [5]. Static friction is essentially also a measure of adhesion, but under predominantly shear loading, and is enhanced by the same mechanism [19, 31]. For a smooth indenter (Fig. 5c), crack-trapping increases the effective work of adhesion by a factor over its value for an unstructured flat elastomer, i.e., $W_{eff} = cW$, in which c is the enhancement ratio, a number (> 1) that depends on the geometrical parameters of the structure [32]. So, the static friction for smooth indenter on film-terminated fibrillar samples is:

$$F_{static,p} = \sqrt{6\pi RW_{eff}} \tag{6}$$

By Eq. (3), the sliding friction for film-terminated fibrillar structures equals the product of sliding shear stress and contact area, i.e., it is more or less the same as that of flat control. For a film-terminated ridge/channel structure, the situation is different because, for sufficiently large spacing between ridges, a new mechanism for energy dissipation, internal friction due to folding [32], is activated and hence

$$F_{\text{sliding,ridge}} = \tau A b \tag{7}$$

where b is a known friction enhancement factor that can be smaller or greater than unity, depending on the spacing.

Case (d) Consider now the case of a rough indenter on a structured surface (film-terminated fibrillar or ridge/channel, Fig. 5d). Figure 3 shows that the crack-trapping mechanism remains operative even for a rough surface. The measured dependence of static friction, pull-off force, and sliding friction can be explained by combining effects discussed in cases (b) and (c). Static friction (Eq. 2) is controlled by the effective work of adhesion, which is changed due to both the structure and the reduction in contact area due to roughness:

$$W_{\text{eff,r}} = \alpha \left(cW - U_{\text{el}} \right) \tag{8}$$

Here, the reduction in effective adhesion due to roughness is captured by α (contact area reduction) and U_{el} (elastic energy due to roughness). The increase in static friction due to crack-trapping is captured by the factor c. Equation (8) predicts a monotonic increase in static friction with actual area of contact, which is consistent with Fig. 3b. A very similar argument applies for adhesion (Eq. 1), as measured by pull-off force. Again, Eq. (8) along with Eq. (1) predicts a monotonic increase in pull-off force with actual area of contact, as observed in Fig. 3c. For the film-terminated ridge/channel samples sliding against a rough indenter, the sliding friction can be approximated as

$$F_{\text{sliding,ridge,r}} = \tau \alpha A b \tag{9}$$

This expresses the idea that sliding friction is enhanced due to subsurface folding and sliding (factor b), and reduced due to partial contact. In actuality, the enhancement factor, b, depends on both the sample structure and also indenter roughness. Equation 9 provides an empirical explanation of the effect of various physical properties on sliding friction for our structured samples. Experimental data shown in Fig. 4 suggests that this simple relation breaks down for small contact areas (those are not represented by the linearly fitted line). In previous work [32], we derived a condition for onset of buckling that is a prerequisite for internal folding. It shows that sliding friction at the indenter-sample surface needs to be above a certain value. For a rough surface, sufficient reduction in contact area will reduce the average

friction to be below the threshold needed for buckling, effectively turning off the internal folding mechanism.

4 Summary and Conclusions

The principal goal of this work has been to examine the effect of roughness on mechanisms for enhanced adhesion, static friction, and sliding friction that rely on film-terminated architectures. We studied film-terminated fibrillar and ridge/channel structures. The film-terminated fibrillar structures exhibit enhancement of adhesion and static friction due to a crack-trapping mechanism. This mechanism remains substantially operative against rough surfaces. The film-terminated ridge/channel surfaces exhibit strong modulation of sliding friction by internal folding and sliding; this mechanism, too, remains operative against rough surfaces. We suggest that scaling relations that explain the effect of roughness on flat elastomers and the effect of structured surfaces against smooth surfaces can be combined to explain static and sliding friction of structured surfaces against rough indenters.

References

1. Takahashi, K., Berengueres, J.O.L., Obata, K.J., Saito, S.: Geckos' foot hair structure and their ability to hang from rough surfaces and move quickly. Int. J. Adhes. Adhes. **26**, 639–643 (2006). doi:10.1016/j.ijadhadh.2005.12.002

2. Autumn, K., Liang, Y.A., Hsieh, S.T., Zesch, W., Chan, W.P., Kenny, T.W., Fearing, R., Full, R.J.: Adhesive force of a single gecko foot-hair. Nature **405**, 681–685 (2000). doi:10.1038/35015073

3. Davies, J., Haq, S., Hawke, T., Sargent, J.P.: A practical approach to the development of a synthetic Gecko tape. Int. J. Adhes. Adhes. **29**, 380–390 (2009). doi:10.1016/j.ijadhadh.2008.07.009

4. Del Campo, A., Greiner, C., Álvarez, I., Arzt, E.: Patterned surfaces with pillars with controlled 3D tip geometry mimicking bioattachment devices. Adv. Mater. **19**, 1973–1977 (2007). doi:10.1002/adma.200602476

5. Glassmaker, N.J., Jagota, A., Hui, C.-Y., Noderer, W.L., Chaudhury, M.K.: Biologically inspired crack trapping for enhanced adhesion. Proc. Natl. Acad. Sci. **104**, 10786–10791 (2007). doi:10.1073/pnas.0703762104

6. Jagota, A., Hui, C.Y.: Adhesion, friction, and compliance of biomimetic and bio-inspired structured interfaces. Mater. Sci. Eng. R Rep. **72**, 253–292 (2011). doi:10.1016/j.mser.2011.08.001

7. Kim, S., Aksak, B., Sitti, M.: Enhanced friction of elastomer microfiber adhesives with spatulate tips. Appl. Phys. Lett. **91**, 221913 (2007). doi:10.1063/1.2820755

8. Gorb, S.N., Varenberg, M., Peressadko, A., Tuma, J.: Biomimetic mushroom-shaped fibrillar adhesive microstructure. J. R. Soc. Interface **4**, 271–275 (2007). doi:10.1098/rsif.2006.0164

9. Wang, Y., Tian, H., Shao, J., Sameoto, D., Li, X., Wang, L., Hu, H., Ding, Y., Lu, B.: Switchable Dry Adhesion with Step-like Micropillars and Controllable Interfacial Contact. ACS Appl. Mater. Interfaces **8**, 10029–10037 (2016). doi:10.1021/acsami.6b01434

10. Zeng, H., Pesika, N., Tian, Y., Zhao, B., Chen, Y., Tirrell, M., Turner, K.L., Israelachvili, J.N.: Frictional adhesion of patterned surfaces and implications for gecko and biomimetic systems. Langmuir **25**, 7486–7495 (2009). doi:10.1021/la900877h

11. Shen, L., Hui, C.Y., Jagota, A.: A two-dimensional model for enhanced adhesion of film-terminated fibrillar interfaces by crack trapping. J. Appl. Phys. (2008). doi:10.1063/1.3035908

12. Arzt, E., Gorb, S., Spolenak, R.: From micro to nano contacts in biological attachment devices. Proc. Natl. Acad. Sci. U. S. A. **100**, 10603–10606 (2003). doi:10.1073/pnas.1534701100

13. Briggs, G.A.D., Briscoe, B.J.: The effect of surface topography on the adhesion of elastic solids. J. Phys. D Appl. Phys. **10**, 2453–2466 (1977). doi:10.1088/0022-3727/10/18/010

14. Huber, G., Gorb, S.N., Hosoda, N., Spolenak, R., Arzt, E.: Influence of surface roughness on gecko adhesion. Acta Biomater. **3**, 607–610 (2007)

15. Chung, J.Y., Chaudhury, M.K.: Roles of discontinuities in bio-inspired adhesive pads. J. R. Soc. Interface **2**, 55–61 (2005). doi:10.1098/rsif.2004.0020

16. Barreau, V., Hensel, R., Guimard, N.K., Ghatak, A., McMeeking, R.M., Arzt, E.: Fibrillar elastomeric micropatterns create tunable adhesion even to rough surfaces. Adv. Funct. Mater. **26**, 4687–4694 (2016). doi:10.1002/adfm.201600652

17. Jagota, A., Bennison, S.J.: Mechanics of adhesion through a fibrillar microstructure. Integr. Comp. Biol. **42**, 1140–1145 (2002). doi:10.1093/icb/42.6.1140

18. Kim, S., Sitti, M.: Biologically inspired polymer microfibers with spatulate tips as repeatable fibrillar adhesives. Appl. Phys. Lett. **89**, 10–13 (2006). doi:10.1063/1.2424442

19. Shen, L., Glassmaker, N.J., Jagota, A., Hui, C.-Y.: Strongly enhanced static friction using a film-terminated fibrillar interface. Soft Matter **4**, 618 (2008). doi:10.1039/b714737f

20. Kasem, H., Varenberg, M.: Effect of counterface roughness on adhesion of mushroom-shaped microstructure. J. R. Soc. Interface **10**, 20130620 (2013). doi:10.1098/rsif.2013.0620

21. Hui, C.-Y., Glassmaker, N.J., Jagota, A.: How compliance compensates for surface roughness in fibrillar adhesion. J. Adhes. **81**, 699–721 (2005). doi:10.1080/00218460500187673

22. Ruffatto III, D., Parness, A., Spenko, M.: Improving controllable adhesion on both rough and smooth surfaces with a hybrid electrostatic/gecko-like adhesive. J. R. Soc. Interface **11**, 20131089 (2014). doi:10.1098/rsif.2013.1089

23. Vajpayee, S., Jagota, A., Hui, C.-Y.: Adhesion of a fibrillar interface on wet and rough surfaces. J. Adhes. **86**, 39–61 (2010). doi:10.1080/00218460903417834

24. Persson, B.N.J.: On the mechanism of adhesion in biological systems. J. Chem. Phys. **118**, 7614–7621 (2003). doi:10.1063/1.1562192

25. Burton, Z., Bhushan, B.: Hydrophobicity, adhesion, and friction properties of nanopatterned polymers and scale dependence for micro- and nanoelectromechanical systems. Nano Lett. **5**, 1607–1613 (2005). doi:10.1021/nl050861b

26. Elleuch, R., Elleuch, K., Ben Abdelounis, H., Zahouani, H.: Surface roughness effect on friction behaviour of elastomeric material. Mater. Sci. Eng. A **465**, 8–12 (2007). doi:10.1016/j.msea.2007.02.127

27. Persson, B.N.J., Tosatti, E.: The effect of surface roughness on the adhesion of elastic solids. J. Chem. Phys. **115**, 5597–5610 (2001). doi:10.1063/1.1398300

28. Persson, B.N.J., Albohr, O., Tartaglino, U.: Volokitin, a I, Tosatti, E.: On the nature of surface roughness with application to contact mechanics, sealing, rubber friction and adhesion. J. Phys. Condens. Matter **17**, R1–R62 (2005). doi:10.1088/0953-8984/17/1/R01

29. Degrandi-Contraires, E., Poulard, C., Restagno, F., Léger, L.: Sliding friction at soft micropatterned elastomer interfaces. Faraday Discuss. **156**, 255 (2012). doi:10.1039/c2fd00121g

30. Pugno, N.M., Lepore, E.: Observation of optimal gecko's adhesion on nanorough surfaces. Biosystems **94**, 218–222 (2008). doi:10.1016/j.biosystems.2008.06.009

31. Shen, L., Jagota, A., Hui, C.: Mechanism of sliding friction on a film-terminated fibrillar interface. Langmuir (2009). doi:10.1021/la803390x

32. He, Z., Hui, C.-Y., Levrard, B., Bai, Y., Jagota, A.: Strongly modulated friction of a film-terminated ridge-channel structure. Sci. Rep. **6**, 26867 (2016). doi:10.1038/srep26867

33. Noderer, W.L., Shen, L., Vajpayee, S., Glassmaker, N.J., Jagota, A., Hui, C.-Y.: Enhanced adhesion and compliance of film-terminated fibrillar surfaces. Proc. R. Soc. A Math. Phys. Eng. Sci. **463**, 2631–2654 (2007). doi:10.1098/rspa.2007.1891

34. Johnson, K.L., Kendall, K., Roberts, A.D.: Surface energy and the contact of elastic solids. Proc. R. Soc. A Math. Phys. Eng. Sci. **324**, 301–313 (1971). doi:10.1098/rspa.1971.0141

35. Savkoor, A.R., Briggs, G.A.D.: The effect of tangential force on the contact of elastic solids in adhesion. Proc. R. Soc. A Math. Phys. Eng. Sci. **356**, 103–114 (1977). doi:10.1098/rspa.1977.0123

36. Chateauminois, A., Fretigny, C.: Local friction at a sliding interface between an elastomer and a rigid spherical probe. Eur. Phys. J. E **27**, 221–227 (2008). doi:10.1140/epje/i2008-10376-5

37. Waters, J.F., Guduru, P.R.: A mechanism for enhanced static sliding resistance owing to surface waviness. Proc. R. Soc. A **467**, 2209–2223 (2011). doi:10.1098/rspa.2010.0617

38. Guduru, P.R.: Detachment of a rigid solid from an elastic wavy surface: theory. J. Mech. Phys. Solids **55**, 445–472 (2007). doi:10.1016/j.jmps.2006.09.004

39. Greenwood, J.A., Williamson, J.B.P.: Contact of nominally flat surfaces. Proc. R. Soc. Lond. A Math. Phys. Eng. Sci. **295**, 300–319 (1966)

40. Greenwood, J.A., Tripp, J.H.: The elastic contact of rough spheres. J. Appl. Mech. **34**, 153 (1967). doi:10.1115/1.3607616

41. Persson, B.N.J.: Theory of rubber friction and contact mechanics. J. Chem. Phys. **115**, 3840 (2001). doi:10.1063/1.1388626